

Spherical Shell Model description of rotational motion

A.P. Zuker*, J. Retamosa**, A. Poves** and E. Caurier*

(*)*Physique Théorique, Bât 40/1 CRN, IN2P3-CNRS/Université Louis Pasteur BP 28, F-67037 Strasbourg Cedex 2, France*

(**)*Departamento de Física Teórica, Universidad Autónoma de Madrid, E-28049 Madrid, Spain*

(September 7, 2018)

Exact diagonalizations with a realistic interaction show that configurations with four neutrons in a major shell and four protons in another —or the same— major shell, behave systematically as backbending rotors. The dominance of the $q \cdot q$ component of the interaction is explained by an approximate form of SU3 symmetry. It is suggested that these configurations are associated with the onset of rotational motion in medium and heavy nuclei.

The SU3 model of Elliott [1] provides a microscopic description of rotors that exhibit spectra in $J(J+1)$. For sufficiently low J , or sufficiently large representations they became perfect in the sense of having a constant intrinsic quadrupole moment $Q_0 = Q_0(J)$, where

$$Q_0(J) = \frac{(J+1)(2J+3)}{3K^2 - J(J+1)} \langle JJ|3z^2 - r^2|JJ \rangle, \quad (1)$$

as postulated in the strong coupling limit of the unified model of Bohr and Mottelson [2].

Since the quadrupole force that appears in the SU3 Casimir operator is also an important part of the nuclear interaction [3,4], we expect it to play a determinant role in the onset of rotational motion in real nuclei - the problem we want to address. A direct approach would demand, in general, diagonalizations in spaces of two major shells in neutrons and protons as first proposed by Kumar and Baranger [5]. Dimensionalities are then of order 10^{40} , exceeding by far what is possible at present (10^7) [6].

Therefore, it is necessary to develop a computational strategy, and our starting point will consist in learning as much as we can from situations in which neutrons and protons are independently restricted to a single major shell, that can be the same close to $N=Z$. The exact results in I will show that rotational features -including the systematic appearance of backbending- are determined by the interplay of the quadrupole force with the central field, in the subspace of a major shell spanned by the sequence of $\Delta j = 2$ orbits that comes lowest under the spin-orbit splitting. This state of affairs is related to the existence of an approximate symmetry (quasi-SU3), introduced in II. The relevance of these results to rotors in medium and heavy nuclei will be explained in III.

NOTATIONS. ν = neutrons, π = protons, $C^{lm} = \sqrt{4\pi/(2l+1)}Y^{lm}$, $q \equiv q^{2m} = r^2C^{2m}$.

p is the principal quantum number, r_p is the generic label for all orbits in the p -th oscillator shell *except* the largest (i.e. $j = j_{\max} = p + 1/2$).

We use l for $j = l + 1/2$ orbits in the sense $h = h_{11/2}$, $g = g_{9/2}$, $p = p_{3/2}$ etc., except in the following

CONVENTION: pfh means the full $p = 5$ shell, i.e. $p_{1/2}, p_{3/2}, f_{5/2}, f_{7/2}, h_{9/2}, h_{11/2}$, while $hfp = h_{11/2}f_{7/2}p_{3/2}$, and similarly for other shells.

I. Exact Results. Although a space of a full major shell, with very specific single-particle spacings, is necessary to ensure strict SU3 symmetry, we know of several examples where the ds or fp subspaces produce rotor-like spectra in the presence of spin-orbit splittings: $(ds)^4$ describes ^{20}Ne quite well [7] and $(ds)^3_\pi(fp)^2_\nu$ configurations explain the onset of deformation in ^{31}Na and ^{32}Mg [8]. Furthermore ^{48}Cr provides the first example of a backbending band in $N=Z$ nuclei. The experimental spectrum [9] is almost perfectly reproduced by a full $(pf)^8$ shell model calculation, with strong indications that the $(fp)^8$ space is sufficient to explain the quadrupole coherence [11]. The situation has a double interest. As we shall explain in III, configurations that consist of 4 protons in a major shell and 4 neutrons in another (the same in $N \approx Z$) play a key role in the onset of rotational motion in heavier nuclei, and the restriction to the $\Delta j = 2$ spaces makes the diagonalizations possible, as illustrated by the four cases we are going to treat (in parenthesis the corresponding m-scheme dimensionalities):

$$\begin{aligned} (fp)^8 T = 0; (2 \times 10^4), & \quad (fp)^4_\pi(gds)^4_\nu; (1.1 \times 10^5), \\ (gds)^8 T = 0; (6 \times 10^5), & \quad (gds)^4_\pi(hfp)^4_\nu; (1.9 \times 10^6), \end{aligned}$$

against

$$\begin{aligned} (pf)^8 T = 0; (2 \times 10^6), & \quad (pf)^4_\pi(sdg)^4_\nu; (10^7), \\ (sdg)^8 T = 0; (5 \times 10^7), & \quad (sdg)^4_\pi(pfh)^4_\nu; (1.9 \times 10^8). \end{aligned}$$

We shall compare the results obtained with the KLS interaction [12] and with a pure quadrupole forces using $\hbar\omega = 9\text{ MeV}$ with a uniform single particle spacing $\varepsilon = 1\text{ MeV}$, corresponding to the standard $-\beta\ell \cdot s$ splitting ($\beta \approx 20A^{-2/3}\text{ MeV}$ and $\hbar\omega \approx 40A^{-1/3}$) [13].

It has been shown in [4] that for one shell the quadrupole component of a general realistic interaction has the form $-e_2\bar{q}_p \cdot \bar{q}_p$, where e_2 goes as $A^{-1/3}$ and, $\bar{q}_p = q_p/\mathcal{N}_p^{(2)}$ is the quadrupole operator q_p in shell p , normalized by $\mathcal{N}_p^{(2)}$ - the square root of the sum of the squares of the matrix elements of q_p - which goes as $(p+3/2)^2$. For two contiguous shells the force is $-e_2(\bar{q}_p + \bar{q}_{p+1}) \cdot (\bar{q}_p + \bar{q}_{p+1})$, with the *same* e_2 coupling, and it differs markedly from the traditional $\chi(q_p + q_{p+1}) \cdot (q_p + q_{p+1})$, with $\chi = O(A^{-5/3})$ [3].

Fig.1 shows the yrast bands in the four spaces. Rotational behaviour is fair to excellent at low J . As expected from the normalization property of the realistic quadrupole force the moments of inertia in the rotational region go as $(p+3/2)^2(p'+3/2)^2$, i.e. if we multiply all the E_γ values by this factor the lines become parallel. The Q_0 values are constant to within 5% up to a critical J value at which the bands backbend.

Since all the spaces behave in the same way we specialize to $(gds)^8$ in what follows. Fig.2 shows the results of diagonalizing $e_2\bar{q}_p \cdot \bar{q}_p$ ($p=4$). At $e_2=9.6$ the ε splittings are overwhelmed and we have a nearly perfect rotor. The value of Q_0 stays practically constant up to $J=16-18$ and then decreases slowly. At $e_2=4.8, 3.2$ and 2.4 the rotational behaviour remains very good below $J=14$. Then there is a break and the upper values are again aligned. At $e_2=3.2$ the overlap of each state with the one obtained with the full KLS interaction is always better than $(0.95)^2$, which suggests that

$$\langle h|\mathcal{H}|h \rangle_J \approx \langle q|\mathcal{H}|q \rangle_J,$$

where $|h \rangle$ and $|q \rangle$ are the eigenstates of the full Hamiltonian \mathcal{H} and the quadrupole force ($e_2=3.2$) respectively. Fig.3 shows that this is the case indeed. It means that the observed backbending pattern is obtained by doing first order perturbation theory on $|q \rangle$: the spectrum changes but not the *structure* (i.e. the wavefunctions). A similar situation is found when comparing the full $(pf)^8$ calculation with a renormalized interaction and $\varepsilon=2$ (fig. 10 of ref. [11]) and the $(fp)^8$ result in fig. 1: the backbend occurs at the same J and the Q_0 values are very close in spite of a much larger slope (i.e., smaller moment of inertia) in the bigger calculation. Here again perturbation theory should operate well.

To gain some insight into the backbending phenomenon we examine the evolution of the wavefunctions and quadrupole moments. In fig.4 we find that for $e_2=9.6$ the percentage of the g^8 configuration in the full eigenstate is very small and nicely correlated with the Q_0 values. This is what we expect from a good rotor, for which the amplitudes of any configuration (not only g^8) must be J -independent (since all states must be projections of the same intrinsic state). For the KLS results and their $e_2=3.2$ counterparts $Q_0(J)$ decreases abruptly above $J=14$, while the g^8 configuration increases its amplitude and becomes dominant in the region where $Q_0(J)$ reaches a plateau. It is clear that at the backbend the notion of intrinsic state loses - or changes - its meaning, and the idea of a band crossing suggested by fig.2 becomes questionable. Work remains to be done to understand the connection of our results with the mean field ones [14].

II. Quasi-SU3. That the build up of quadrupole coherence needs only the lower $\Delta j=2$ sequence of the full shell can be understood by examining table 1 where we list the matrix elements of $q^{20} = r^2 C^{20} = \frac{1}{2}(3z^2 - r^2)$, in jj and LS coupling. It is seen that the $\Delta j=1$ matrix elements are small, both for m small (prolate shapes) and m large (oblate). If we simply neglect them, diagonalizing the $\Delta j=2$ matrix in jj scheme is very much equivalent to diagonalizing the exact q^{20} operator in LS scheme. This amounts to saying that the sequence $j=1/2, 5/2, 9/2 \dots$ (or $j=3/2, 7/2, 11/2 \dots$) must behave very much as an $l=0, 2, 4 \dots$ (or $l=1, 3, 5 \dots$) one. Therefore we introduce a new operator (the 'quasi' q^{20}), defined in the $\Delta j=2$ space via the following replacements in the LS matrix elements of q^{20} : $l \rightarrow j, p \rightarrow p+1/2, m \rightarrow m+1/2$ and $-m \rightarrow -m-1/2$: ($m > 0$).

In fig.5 we draw to the left the spectrum of the full q^{20} operator (in fact $2q^{20}$), i.e., the SU3 Nilsson orbits. The band-heads come at $2(p+3/4-3/2|m|)$. To the right we have plotted the spectrum of the 'quasi' $2q^{20}$ operator. Now the band-heads are at $2(p+1/2-3/2|m|)$, that is, the exact LS values, except for $m=\pm 1/2$, where the one to one correspondence between the "quasi" q^{20} and the exact q^{20} in LS scheme breaks down. The corresponding "quasi-SU3" symmetry cannot be exact because of this mismatch. Notice however that the mismatch is very small ($< 1\%$). The spectrum of the true q^{20} operator in the $\Delta j=2$ space is extremely close to the one in fig. 5, and it is clear that the amount of quadrupole coherence obtained by filling the m (or K) = 1/2 and 3/2 orbits is almost as large as for the SU3 orbitals. For the eight particle blocks we are interested in, the intrinsic Q_0 would be

$$Q_0 = 8[e_\pi(p_\pi - 1) + e_\nu(p_\nu - 1)] \quad (2)$$

For $p_\pi = 5, p_\nu = 6$ and effective charges $e_\pi = 1.5, e_\nu = 0.5$, we have $Q_0 = 68$ (in dimensionless oscillator coordinates, i.e., $r \rightarrow r/b$ with $b \approx A^{-1/6}fm$), which is related to the $E2$ transition probability from the ground state by

$B(E2) \uparrow = 10^{-5} A^{2/3} Q_0^2 = 1.4 e^2 b^2$ for $A = 166$. We shall see soon the relevance of this number. The Q_0 values obtained in I with the $q \cdot q$ interaction at $e_2 = 9.6$ saturate the value predicted by eq.2 within 2% while at $e_2 = 2.4$ we still have 80% of this limit.

III. The onset of rotation.

Fig.6 proposes a schematic view of the single particle order expected around $Z = 50, N = 82$ closure. *Mutatis mutandis*, the same scheme applies to the $Z = 28, N = 50$ and $Z = 82, N = 126$ closures. For the lower shells we have a conventional sequence, and for the upper (empty) ones we have assumed a spin orbit splitting, which may be naive, but it is correct in the light nuclei and consistent with the (scarce) available data in the heavier ones .

Nilsson diagrams [15,16] predict that when nuclei acquire a stable deformation, two orbits $K = 1/2$ and $3/2$ – originating in the upper shells of fig. 5 – become occupied. This result is common to different regions and to different calculations and provides a strong clue that we turn upside down when translating it into spherical language as: *Rotational motion sets in when 8 particles are promoted to the $(p f h)_{\pi}^4 (s d g i)_{\nu}^4$ configuration*, suggesting that the calculations we have presented may be the first step in implementing a shell model view of real rotors. The $BE2$ estimate at the end of the previous section is a factor four smaller than the largest observed values in the region [17]. It means that Q_0 is only a factor two too small. Therefore the lower orbits should supply the missing half, which is very plausible because their potential quadrupole coherence is high. The reason is that the r_p groups in fig. 6 are pseudo-oscillator shells with $p' = p - 1$ and the pseudo-SU3 symmetry of Arima, Draayer, Harvey and Hecht (and hence the left part of fig. 5) would provide the relevant coupling scheme (ref. [18] contains a recent survey of pseudo-SU3). It should be noted that the quadrupole coherence in the upper(u) and lower(l) spaces is mutually reinforced through coupling terms of the form $-e_2 \bar{q}_u \cdot \bar{q}_l$.

Conclusions. The zeroth order approximation we are proposing for rotational nuclei is very similar to the weak coupling explanation of the famous 4p-4h low lying states in ^{16}O and ^{40}Ca . The differences are that in the heavier nuclei they become ground states, as in ^{80}Zr , and most probably 8p-8h excitations are necessary to ensure the observed quadrupole coherence. The fact that the calculations naturally produce backbending in the upper configurations (which are the driving ones, as in light nuclei) indicates that we are closer to real rotors than to idealized constructions. The tendency of quadrupole forces of Elliott type to produce clustering in the excited states [19,20] will probably lead to significant differences of interpretation between the spherical and deformed formulations for large quadrupole moments.

This work is supported in part by the IN2P3 (France)-CICYT (Spain) agreements and by grant DGICYT PB93-263 (Spain).

- [1] J.P. Elliott *Proc. Roy. Soc.* **245** 128,562 (1956)
- [2] A. Bohr and B. Mottelson, *Math. Fis. Medd. Dan. Vid. Selsk* **27** no 16 (1953)
- [3] M. Baranger and K. Kumar *Nucl. Phys.* **A110**, 490 (1968)
- [4] M. Dufour and A.P. Zuker, submitted to *Phys. Rev. Lett.* and preprint CRN 93-29, 1993, Strasbourg
- [5] K. Kumar and M. Baranger *Nucl. Phys.* **A110**, 529 (1968)
- [6] ANTOINE code, CRN, Strasbourg 1989, to be released
- [7] A. Arima, S. Cohen, R.D. Lawson and M. McFarlane *Nucl. Phys.* **A108** 94 (1968)
- [8] A. Poves and J. Retamosa *Nucl. Phys.* **A571**, 221 (1994)
- [9] J.A. Cameron *et al.*, *Phys. Lett.* **319B** 58 (1993)
- [10] A. Abouzouzi, E. Caurier and A.P. Zuker *Phys. Rev. Lett.* **66**, 1134 (1991) , and in preparation.
- [11] E. Caurier, A.P. Zuker, A. Poves and G. Martinez-Pinedo, *Phys. Rev.* **C50**, 225 (1994)
- [12] S. Kahana, H.C. Lee and C.K. Scott *Phys. Rev.* **180**, 956 (1969) ; *Phys. Rev.* **185**, 1378 (1969)
- [13] A. Bohr and B. Mottelson Nuclear Structure vols I (Benjamin, 1964)
- [14] J. L. Egido and L. M. Robledo, *Phys. Rev. Lett.* **70**, 2876 (1993)
- [15] S.G. Nilsson *Mat. Fys. Medd. Dan. Vid. Selsk.* **29**, 1 (1955)
- [16] A.K. Jain, R.K. Sheline, P.C. Wood and K. Jain *Rev. Mod. Phys.* **62** 393 (1990)
- [17] S. Raman, C.W. Nestor and K.H. Bhatt *Phys. Rev.* **C37**, 805 (1988)
- [18] J.P. Draayer in Future Directions in Nuclear Physics with $4\pi\gamma$ Detectors (J.Dudek and B. Haas eds A.I.P. 1992)
- [19] D.M. Brink in Course XXXVI Enrico Fermi School, C. Bloch editor (Academic Press, 1966)
- [20] Y. Abgrall, G. Baron, E. Caurier and G. Monsonego, *Phys. Lett.* **24B**, 609 (1967); *Phys. Lett.* **26B**, 53 (1967)

TABLE I. The matrix elements of r^2 and C_{20} in jj and LS coupling

$\langle pl r^2 pl \rangle = p + 3/2$	$\langle pl r^2 pl + 2 \rangle = -[(p-l)(p+l+3)]^{1/2}$
$\langle jm C_2 jm \rangle = \frac{j(j+1) - 3m^2}{2j(2j+2)}$	$\langle lm C_2 lm \rangle = \frac{l(l+1) - 3m^2}{(2l+3)(2l-1)}$
$\langle jm C_2 j+1m \rangle = -\frac{3m[(j+1)^2 - m^2]^{1/2}}{(2j+4)(2j+2)(2j)}$	
$\langle jm C_2 j+2m \rangle = \frac{3}{2} \left\{ \frac{[(j+2)^2 - m^2][(j+1)^2 - m^2]}{(2j+2)^2(2j+4)^2} \right\}^{1/2}$	$\langle lm C_2 l+2m \rangle = \frac{3}{2} \left\{ \frac{[(l+2)^2 - m^2][(l+1)^2 - m^2]}{(2l+5)(2l+3)^2(2l+1)} \right\}^{1/2}$

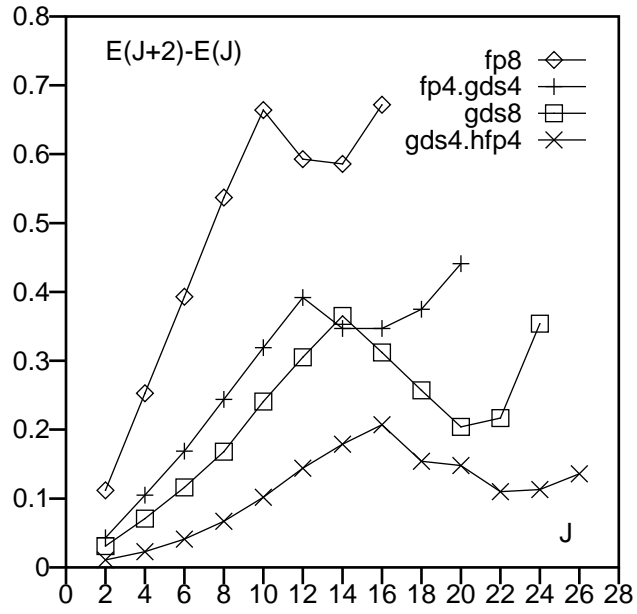


FIG. 1. Yrast transition energies $E_\gamma = E(J+2) - E(J)$ for different configurations, KLS interaction.

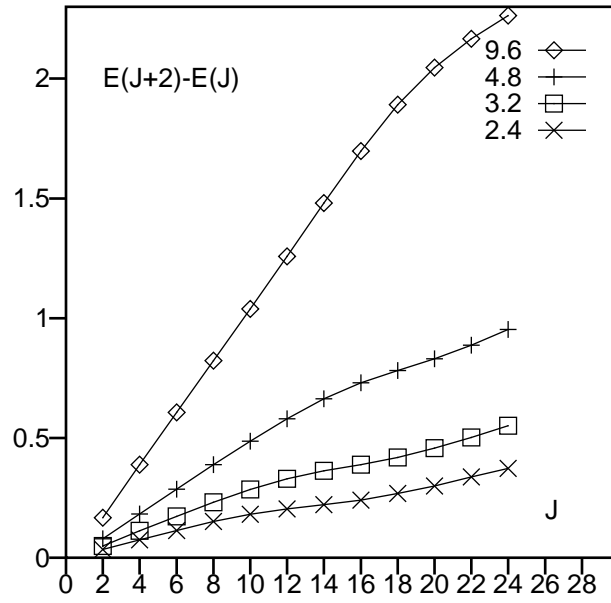


FIG. 2. Yrast transition energies $E_\gamma = E(J+2) - E(J)$ for the $(gds)^8$ configuration with an $-e_2\bar{q} \cdot \bar{q}$ force.

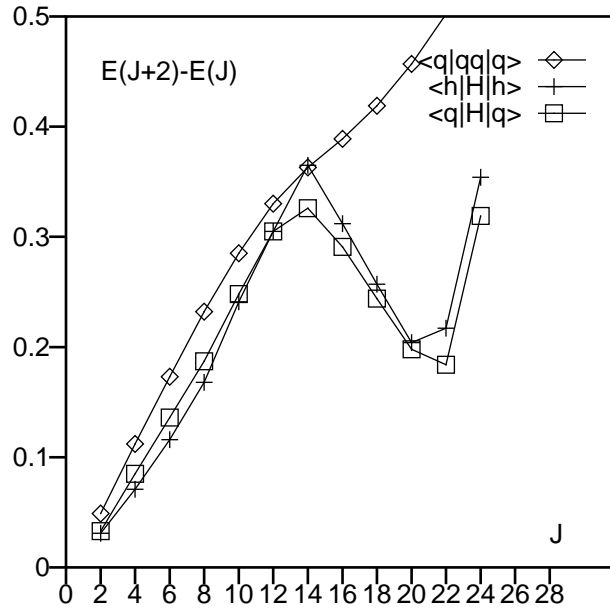


FIG. 3. $\langle h|H|h \rangle = (gds)^8$ in fig. 3; $\langle q|qq|q \rangle = 3.2$ in fig. 4 compared with $\langle q|H|q \rangle$. See text.

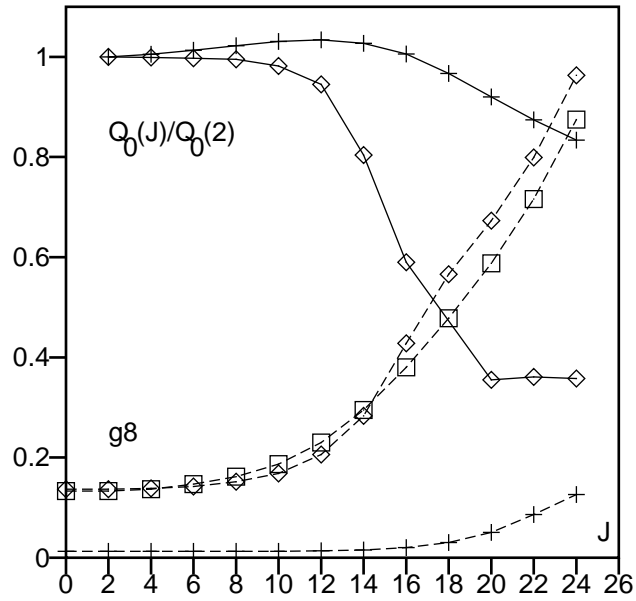


FIG. 4. $Q_0(J)/Q_0(2)$ (full lines) and $g_8 = \langle g^8 | (gds)^8 \rangle^2$ (dashed lines). Wavefunctions calculated with $-e_2 \bar{q} \cdot \bar{q}$ (crosses $\equiv e_2 = 9.6$, squares $\equiv e_2 = 3.2$) and KLS (diamonds).

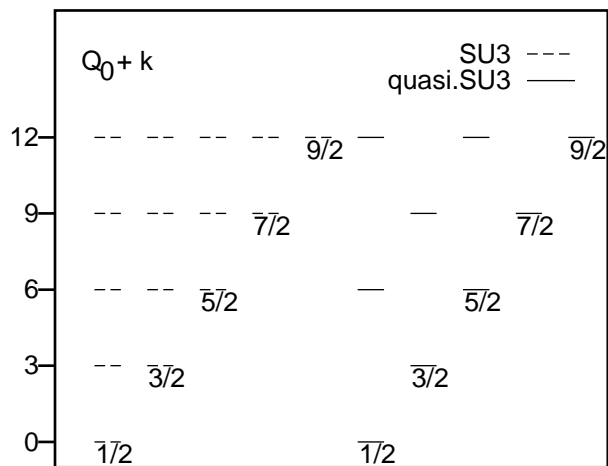


FIG. 5. Nilsson orbits for SU3 ($k = 2p$) and quasi-SU3 ($k = 2p - 1/2$).

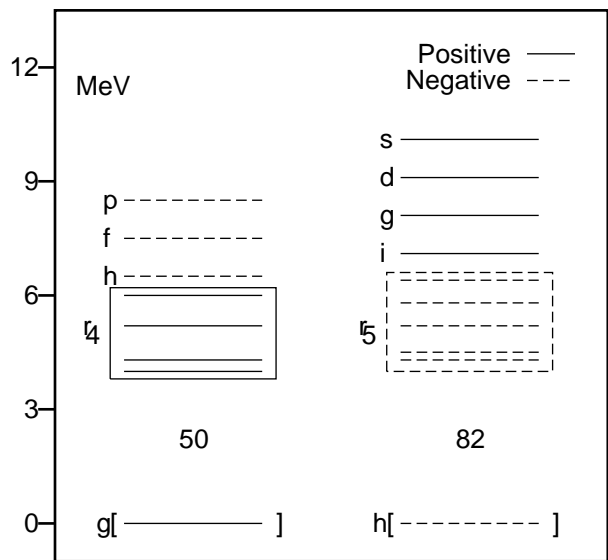


FIG. 6. Schematic single particle spectrum above ^{132}Sn .